Magnetic Resonance in Medicine 59:19–27 (2008)

^{19}F NMR In Vivo Spectroscopy Reflects the Effectiveness of Perfusion-Enhancing Vascular Modifiers for Improving Gemcitabine Chemotherapy

Greg O. Cron,[1] Nelson Beghein,[1] Réginald Ansiaux,[1] Philippe Martinive,[2] Olivier Feron,[2] and Bernard Gallez[1]*

Nuclear magnetic resonance spectroscopy of fluorine-19 (^{19}F NMR) has proven useful for evaluating kinetics of fluorinated chemotherapy drugs in tumors in vivo. This work investigated how three perfusion-enhancing vascular modifiers (BQ123, thalidomide, and Botulinum neurotoxin type A [BoNT-A]) would affect the chemotherapeutic efficacy of gemcitabine, a fluorinated drug widely used in human cancer treatment. Murine tumor growth experiments demonstrated that only BoNT-A showed a strong trend to enhance tumor growth inhibition by gemcitabine (1.7 days growth delay, $P = 0.052$, Student *t*-test). In accord with these results, ^{19}F NMR experiments showed that only BoNT-A increased significantly the uptake of gemcitabine in tumors (50% increase, $P = 0.0008$, Student *t*-test). Further experiments on gemcitabine kinetics (NMR vs time) and distribution (^{19}F MRI) confirmed the uptake-enhancing properties of BoNT-A. The results of this study demonstrate that ^{19}F NMR can monitor modulation of the pharmacokinetics of fluorinated chemotherapy drugs in tumors. The results also show that ^{19}F NMR data can give a strong indication of the effectiveness of perfusion-enhancing vascular modifiers for improving gemcitabine chemotherapy in murine tumors. ^{19}F NMR is a promising tool for preclinical evaluation of such vascular modifiers and may ultimately be used in the clinic to monitor how these modifiers affect chemotherapy. Magn Reson Med 59:19–27, 2008.
© 2007 Wiley-Liss, Inc.

Key words: fluorine NMR; cancer; BQ123; thalidomide; Botox

Nuclear magnetic resonance spectroscopy of fluorine-19 nuclei (^{19}F NMR) has proven to be a useful tool for investigating noninvasively the pharmacokinetics of fluorinated chemotherapy drugs in tumors in vivo (1–4). ^{19}F NMR experiments performed on humans (5–7) and animals (8–23) have found significant correlations between cancer treatment success, normal tissue toxicity, the presence or absence of externally administered biological modifiers (e.g., carbogen), and the uptake and elimination of fluorinated chemotherapy drugs in tumors and normal tissues.

Until now, most such ^{19}F NMR studies have focused on the chemotherapy drug 5-fluorouracil. Only a small number of studies have dealt with the newer fluorinated chemotherapy drug gemcitabine (21,22). Moreover, to our knowledge, no ^{19}F NMR study has been performed using a biological modifier that acts directly on tumor vasculature to enhance the perfusion (delivery) of the chemotherapy drug. In the context of cancer treatment, this approach is being pursued actively in preclinical models (24) and in the clinic (25) to enhance the delivery of chemotherapeutic agents and increase the efficacy of the treatment. In our laboratory, we have been experimenting with three such perfusion-enhancing vascular modifiers (BQ123, thalidomide, and Botulinum neurotoxin type A [BoNT-A]), with the goal of increasing tumor perfusion transiently to boost the effectiveness of radiotherapy and chemotherapy (26–30). BQ123 is an endothelin receptor antagonist that induces tumor vessel dilation by blocking the effect of endothelin-1 (ET-1), a very active vasoconstrictor released by tumor cells (26). Thalidomide, an antiangiogenic agent, has recently been shown to increase tumor blood flow transiently by means of a phenomenon referred to as "normalization" of the tumor vasculature (pruning away of less functional vessels) (27–29). BoNT-A has been demonstrated to open up tumor vasculature (i.e., open previously constricted or closed vessels) by decreasing vascular tone (30). These three compounds are possible candidates for clinical use in combination with cytotoxic therapies. Agents that inhibit endothelin-1 receptors have already been used in clinical trials for prostate cancer (31,32). Thalidomide is one of the most studied antiangiogenic agents in clinical trials, including usage in combination with chemotherapeutic agents (33). Finally, BoNT-A has been widely used in the clinic with a long-term established absence of toxicity (absence of systemic effects) when used appropriately (34). Thus, it is certainly valid to envision clinical trials with local administration of BoNT-A in easily accessible tumors.

The original purpose of this work was to test how those three vascular modifiers would affect gemcitabine chemotherapy. After some murine tumor growth experiments (described below), we found that only BoNT-A enhanced

[1]Laboratory of Biomedical Magnetic Resonance and Laboratory of Medicinal Chemistry and Radiopharmacy, Université Catholique de Louvain, UCL, Brussels, Belgium.

[2]Unit of Pharmacology and Therapeutics, Université Catholique de Louvain, UCL, Brussels, Belgium.

Grant sponsor: the Belgian National Fund for Scientific Research (FNRS); Grant sponsor: the Fonds Joseph Maisin; Grant sponsor: the Saint-Luc Foundation; Grant sponsor: the "Actions de Recherches Concertées-Communauté Française de Belgique-ARC"; Grant number: 04/09-317; Grant sponsor: the "Pôle d'attraction Interuniversitaire PAI VI"; Grant number: P6/38.

Dr. Cron's present address is Magnetic Resonance Imaging, Ottawa Health Research Institute, 501 Smyth Road, Ottawa, ON, K1H 8L6 Canada.

*Correspondence to: Bernard Gallez, CMFA/REMA, Avenue Mounier 73.40, B-1200 Brussels, Belgium. E-mail: gallez@cmfa.ucl.ac.be

Received 27 April 2007; revised 5 October 2007; accepted 7 October 2007.
DOI 10.1002/mrm.21469
Published online 29 November 2007 in Wiley InterScience (www.interscience.wiley.com).

© 2007 Wiley-Liss, Inc.

significantly gemcitabine chemotherapy. To gain some understanding of these results, we then used ^{19}F NMR in vivo to measure the effect of the modifiers on the uptake of gemcitabine in the tumors. For the modifier that had the most spectacular effect (BoNT-A), we performed further ^{19}F NMR experiments to study gemcitabine elimination and distribution (the latter through ^{19}F MR imaging).

MATERIALS AND METHODS

All experiments were performed according to national animal care regulations. Intramuscular hepatomas were implanted in the gastrocnemius muscle of the right hind limb of male NMRI (Naval Marine Research Institute) mice (~30–35 g, Janvier) (35). These tumors are hypoxic (oxygen partial pressure < 5 mmHg) and poorly perfused (typically less than half of tumor volume with measurable perfusion), thus mimicking cancers in the clinic that are highly resistant to radiation therapy and chemotherapy. Five different groups of these tumors were grown (on different dates), for a total of 124 tumors (Table 1). Tumor diameters (anterior–posterior axis) were measured manually using calipers (26–28,30). To maximize consistency, the same experimenter (G.O.C.) performed all diameter measurements. Treatments for a given tumor were begun on "day 0," when the tumor had reached a diameter of ~6 mm. The diameter of the tumors on day 2 was 8.0 ± 0.1 mm (numbers given as mean ± SEM unless otherwise stated). Based on T_2-weighted imaging of the mice used for NMR/MRI (groups 2 through 5 in Table 1), the three-dimensional volume of the tumors on day 2 was 0.85 ± 0.03 cm^3. Previously acquired (unpublished) MRI data in our laboratory relating the volume of these tumors to manually measured anterior–posterior diameter indicate that a diameter of 6 mm corresponds to a tumor volume of approximately 0.55 cm^3 (15 mm corresponds to ~2.7 cm^3). In Table 1, "DMSO" refers to an intraperitoneal (i.p.) injection of 100 μL dimethyl sulfoxide (DMSO); "BQ123" refers to an i.p. injection of 1 mg/kg BQ123 (Sigma, Bornem, Belgium); "thal." refers to an i.p. injection of 200 mg/kg racemic thalidomide (Sigma-Aldrich, Bornem, Belgium) dissolved in a volume of 100 μL of DMSO; "BoNT-A" refers to an intratumoral injection of Botulinum neurotoxin type A (BoNT-A; Botox®, Allergan, Antwerp, Belgium; 2 injections of 20 μl at different sites, corresponding to a total dose of 29 U kg^{-1}); and "gemci." refers to an i.p. injection of gemcitabine (Gemzar®, Eli Lilly) at 5 mg/kg for group 1, 800 mg/kg for groups 2–4, and 1600 mg/kg for group 5. "BQ123+gemci." indicates that BQ123 was administered at the same time as gemcitabine (separation < 2 min). A dash "-" indicates no treatment or a sham treatment with saline solution. It should be noted that, when a treatment was performed on a mouse, the treatment was only administered once on the given day. The scheduling, doses, and routes of administration of BQ123, thalidomide, and BoNT-A followed those of previously published work and have been shown to increase tumor perfusion significantly (26–28,30).

For NMR and MR imaging experiments, animals were anesthetized by inhalation of isoflurane mixed with air in a continuous flow (1.8 l/h), delivered by a nose cone. Anesthesia was initiated with 3% isoflurane, then stabilized at ~1.5% isoflurane for 10 min before any manipulation. Animals were maintained at 37°C in the MRI scanner by flushing warm air inside the bore.

Table 1
Tumor Groups and Corresponding Treatments

	Tumor growth experiments (n = 70 total)			
	n	day 0	day 1	day 2
group 1	9	–	–	–
	7	DMSO	DMSO	–
	9	thal.	thal.	–
	10	BoNT-A	–	–
	10	–	–	gemci.
	5	–	–	BQ123 + gemci.
	11	thal.	thal.	gemci.
	9	BoNT-A	–	gemci.
	Initial uptake experiments (n = 45 total)			
	n	day0	day 1	day 2
group 2	9	–	–	gemci.
	9	–	–	BQ123 + gemci.
group 3	5	DMSO	DMSO	gemci.
	6	thal.	thal.	gemci.
group 4	8	–	–	gemci.
	8	BoNT-A	–	gemci.
	Kinetics experiments (n = 6 total)			
	n	day 0	day 1	day 2
subset of group 4	3	–	–	gemci.
	3	BoNT-A	–	gemci.
	^{19}F imaging experiments (n = 9 total)			
	n	day 0	day 1	day 2
group 5	4	–	–	gemci.
	5	BoNT-A	–	gemci.

Tumor Growth Experiments

A group of 70 tumors was prepared for growth experiments (group 1 in Table 1). This group was subdivided into eight subgroups of tumors, each subgroup receiving a different treatment regimen shown by the table. The gemcitabine dose of 5 mg/kg used for this group was chosen after performing separate tumor growth experiments (data not shown) to investigate the efficacy of different doses of gemcitabine varying from 0 to 100 mg/kg. Those experiments showed that 5 mg/kg was below the efficacy threshold for this product, which ensured that any improvements in efficacy conferred by the biological modifiers (BQ123, thalidomide, BoNT-A) would be reflected in the growth curves. After treatments were performed on days 0–2, each tumor was allowed to grow until it reached a diameter of 15 mm (volume ~2.7 cm^3), at which point the mouse was killed. The time to grow from 8 mm (volume ~0.85 cm^3) (on day 2) to 15 mm (volume ~2.7 cm^3) was recorded for each tumor. Differences in this growth time between the different subgroups were assessed by means of the Student *t*-test.

^{19}F and ^{1}H NMR Spectroscopy of Gemcitabine

Implementation of Spectroscopy and Phantom Validation

MR imaging and spectroscopy experiments were performed with a Bruker Biospec 4.7T MRI scanner (Karlsruhe, Ger-

many) and a 25-mm diameter surface coil that could be tuned separately to either ^{1}H (200.1 MHz) or ^{19}F (188.3 MHz). Preliminary experience showed that the tumor ^{19}F signal of gemcitabine (administered i.p. to the mouse) was very small (gemcitabine spectrum height divided by standard deviation of noise was less than 5 for a gemcitabine dose of 100 mg/kg, 150 averages, repetition time = 6 s). Thus, every possible effort was made to maximize the ^{19}F signal-to-noise ratio (SNR). NMR spectroscopy was performed in a nonlocalized manner (simple excite–acquire pulse sequence) to sample the earliest possible time points of the free induction decay (FID) and thereby increase spectra SNR. For mouse tumor experiments, the surface coil was placed directly on the tumor in such a way as to maximize the NMR signal received from the tumor and minimize the signal from the upper leg and paw. The tail and non–tumor-bearing left hind limb were positioned completely outside the sensitive volume of the coil. A small, sealed glass capillary tube containing a small sample of hexafluorobenzene was permanently affixed to the underside of the coil. This procedure provided a consistent ^{19}F signal easily distinguishable from gemcitabine (~51 ppm downfield from gemcitabine) which was used for quality assurance purposes (more details given at the end of this section). As has been the case in previous work, the gemcitabine parent compound and metabolites were not distinguishable in the ^{19}F spectra (21,22). Thus, gemcitabine was treated as a single peak. ^{1}H and ^{19}F spectroscopy were performed with the following parameters: excitation angle = 90°, spectral width = 25 kHz, acquisition size = 8k, repetition time = 6 s (to ensure complete relaxation). For ^{1}H spectroscopy, an 80-μs-long block radio frequency (RF) excitation pulse was used, whereas for ^{19}F spectroscopy a 20-μs-long block pulse was used. Four averages were acquired for ^{1}H spectroscopy, whereas 150 averages were acquired for ^{19}F spectroscopy (total ^{19}F acquisition time = 15 min). The frequency of the RF excitation pulse was centered directly on the water peak for ^{1}H spectroscopy and ~7 ppm downfield of the gemcitabine peak for ^{19}F spectroscopy. FIDs were Fourier transformed (exponential line broadening 25 Hz for ^{19}F spectra), phased, and baseline corrected. The real part of each spectrum was integrated over the water peak for ^{1}H spectroscopy (integration width = 20 ppm) and over the gemcitabine peak for ^{19}F spectroscopy (integration width = 12 ppm). Each integral was divided by the receiver gain number used for that acquisition. (The receiver gain for ^{19}F spectroscopy was always set to the same value, which was the maximum possible for the scanner.) A relative measure of the concentration of gemcitabine measured by spectroscopy ($[gem]_{rel}$) was then obtained by dividing the gemcitabine integral by the water integral.

Ten aqueous ~1-ml plastic centrifuge tubes were prepared with known concentrations of gemcitabine (range, 0–3 mM). These phantoms were used to test the reproducibility and linearity of $[gem]_{rel}$ as a function of gemcitabine concentration. $[gem]_{rel}$ measurements with these phantoms were found to be linear with gemcitabine concentration ($R = 0.99$) with a slope of 0.135 mM^{-1}. $[gem]_{rel}$ measurements were henceforth multiplied by the inverse of that slope, 7.41 mM, so that the numerical values of $[gem]_{rel}$ would be approximately equal to the absolute concentrations of gemcitabine in mM. The equality between $[gem]_{rel}$ and absolute concentration is only approximate, because it assumes uniform distribution of gemcitabine, homogeneous unit density of tissue, and no NMR-invisible ^{1}H or ^{19}F nuclei. $[gem]_{rel}$ measurements were found to be reproducible to within < 10% (~0.16 mM), even when the phantoms were completely removed from the scanner and put back in with different geometrical orientations (necessitating new shimming). For repeat measurements on the same phantom (not removed from the scanner), the reproducibility improved to < 7% (~0.11 mM).

For the in vivo ^{19}F spectroscopy data, the integral of the real part of the spectrum peak corresponding to the hexafluorobenzene reference tube (integration width = 18 ppm) was very stable from experiment to experiment, varying by less than 7.5% of the mean for all studies (standard deviation = 3.7% of the mean). The positions (in frequency) of the gemcitabine and hexafluorobenzene peaks were very stable as well (7.3 ± 0.2 ppm for gemcitabine, −43.5 ± 0.6 ppm for hexafluorobenzene, mean ± standard deviation, transmitter frequency = 188.2805 MHz). Thus, from a quality assurance viewpoint, we considered that all our spectroscopy data were valid.

Initial Uptake in Tumors In Vivo

Three separate groups of tumors were prepared for NMR experiments investigating the initial uptake of gemcitabine in tumors (groups 2, 3, and 4 in Table 1). Each of these groups was divided into a control subgroup (gemcitabine only) and a treatment subgroup (gemcitabine + modifier). On day 2, gemcitabine (800 mg/kg) was injected i.p. into the awake mouse in a fume hood facility approved for the handling of chemotherapeutic agents. The dose of 800 mg/kg provided gemcitabine concentrations in the tumor of ~1–2 mM. This dose was chosen to ensure adequate SNR and reproducibility for ^{19}F spectroscopy. Preliminary in vivo ^{19}F spectroscopy tumor experiments with gemcitabine doses of 100, 200, 400, and 800 mg/kg had given SNRs (gemcitabine spectrum height divided by standard deviation of baseline noise) of approximately 4, 6, 13, and 25, respectively (same 15-min acquisition described above). Our technical goal was an SNR of at least 20 for a 15-min acquisition (repetition time = 6 s), leading to our choice of the 800 mg/kg dose. This dose is within the range of single-dose chemotherapy experiments which have been performed safely by other investigators (i.e., no acute [~hours] toxicity) (36).

After gemcitabine administration, the mouse (under isoflurane anesthesia) was transported to the MRI facility and installed in the MRI scanner. The surface coil was initially set to ^{1}H mode for shimming, preliminary imaging (to check positioning), and ^{1}H spectroscopy. Immediately afterward, the coil was set to ^{19}F mode and one spectroscopy acquisition was begun. This acquisition commenced 37.5 min after the i.p. injection of gemcitabine and finished 52.5 min after the injection (15-min acquisition). Thus, the mean acquisition time post-i.p. was considered to be 45 min (= the mean of 37.5 and 52.5 min). After the end of the ^{19}F acquisition, the coil was switched back to ^{1}H mode for multislice proton-density and T_2-weighted imaging of the tumor. For proton density-weighted imaging, a gradient echo pulse sequence was used with field of view (FOV) = 40 mm, matrix = 64 × 64, 20 transverse (axial)

slices, slice thickness = 2 mm, repetition time = 5 s, echo time = 4.5 ms, and flip angle = 90°. For T_2-weighted imaging, a fast spin echo pulse sequence was used with FOV = 40 mm, matrix = 128 × 128, 20 transverse (axial) slices, slice thickness = 2 mm, repetition time = 4 s, and effective echo time = 50 ms.

For each tumor, the ^{1}H and ^{19}F spectroscopy data were used to compute the value of $[gem]_{rel}$ 45 min post-i.p. injection of gemcitabine. For each tumor group (i.e., groups 2, 3, and 4 in Table 1), all $[gem]_{rel}$ values were normalized to the average value found for the control subgroup. This was done to facilitate comparisons between groups. For each tumor group, $[gem]_{rel}$ values for the control subgroup were compared with values for the treatment subgroup by means of the Student *t*-test.

Nonlocalized spectroscopy measurements gather NMR signals not only from the tumor, but also from adjacent muscle, fat, skin, and any other structure that is within the sensitive volume of the surface coil. The proton-density and T_2-weighted images were used to estimate the percentage of total NMR signal produced by the tumor alone, to rule out any biases in the data that could be caused by variations in tissue composition. Regions of interest (ROIs) were drawn around the tumor on the T_2-weighted images. These ROIs were then used to compute the percentage of total MRI signal in the proton-density–weighted images contributed by the tumor.

For five mice in each subgroup of group 4 (BoNT-A experiments), ~1 ml of blood was withdrawn by means of cardiac puncture at the end of the experiment (60 min post-i.p. injection of gemcitabine). The blood was placed in a plastic heparinized centrifuge tube, and a $[gem]_{rel}$ measurement was performed in the scanner to obtain an estimate of the concentration of gemcitabine in the blood. This procedure was to verify that any differences in tumor $[gem]_{rel}$ between the control and treatment subgroups were not due simply to differences in gemcitabine blood concentration.

Kinetics in Tumors In Vivo (BoNT-A Experiments)

Six tumors (three controls, three treated with BoNT-A) from group 4 were used to investigate $[gem]_{rel}$ as a function of time. The protocol and analysis were similar to the initial uptake experiments, except that 16 sequential ^{19}F acquisitions were performed instead of 1. Additionally, a maximum possible effort was made to perform the initial steps of the protocol quickly (transportation of the mouse, installation in the scanner, and so on), which allowed the mean acquisition time post-i.p. of the first ^{19}F spectrum to be 30 min (start of acquisition = 22.5 min, end of acquisition = 37.5 min) instead of the usual mean acquisition time of 45 min. For each tumor, the ^{1}H and ^{19}F spectroscopy data were used to compute the value of $[gem]_{rel}$ as a function of time post-i.p. injection of gemcitabine. Here, $[gem]_{rel}$ values were not normalized to the control subgroup. These $[gem]_{rel}$ vs time data were then used to compute the area under the curve (AUC, for all time points) and the slope of the elimination phase of the curve (linear regression performed on time points > 120 min).

^{19}F MR Imaging of Gemcitabine in Tumors In Vivo

^{19}F MR imaging of gemcitabine was performed on a group of nine tumors (four control, five treated with BoNT-A, group 5 in Table 1). The protocol was similar to that used for the spectroscopy experiments. The gemcitabine dose used for ^{19}F imaging was 1600 mg/kg instead of 800 mg/kg. This doubling of the dose used for spectroscopy was deemed necessary after preliminary experiments showed that the ^{19}F image SNR would not be adequate with 800 mg/kg. To our knowledge, 1600 mg/kg administered to a mouse is greater than any single dose that has ever been used by other investigators. Thus, to ensure a lack of acute (~hours) toxicity, a separate group of five mice (not included in Table 1) was injected with that dose and observed for 24 hr. No deaths, weight loss, or adverse behavioral effects were observed for that time period.

For the ^{19}F imaging experiments, after the mice were installed in the MRI scanner, the ^{1}H mode of the surface coil was used for shimming and preliminary imaging (to check positioning). The coil was then switched to ^{19}F mode. One ^{19}F spectrum was acquired to find the precise center frequency of the gemcitabine peak. Using this as the center transmit frequency, a ^{19}F gradient echo imaging pulse sequence was then commenced. This pulse sequence acquired a single projection image (i.e., ~infinite slice thickness) in the coronal plane. Other parameters were as follows: FOV = 70 mm, matrix = 32 × 32, repetition time = 6 s, echo time = 2.1 ms, flip angle = 90°, number of averages = 16, total acquisition time = 51 min. A gaussian RF pulse shape with length 680 μs was used for excitation. This pulse had no significant spectral power at frequencies farther than ~5 kHz from the center frequency. This ensured that the ^{19}F signals from the isoflurane anesthetic (~6.4 kHz upfield of the gemcitabine peak) and the hexafluorobenzene sample (~9.6 kHz downfield) would not contaminate the gemcitabine images. The time between the i.p. injection of gemcitabine and the midpoint of the ^{19}F image acquisition was 62 min.

After ^{19}F imaging, the coil was switched back to ^{1}H mode. A proton-density–weighted projection image was acquired, whose pulse sequence was nearly identical to the one used for ^{19}F imaging (except 2 averages and center frequency set to the water peak). Finally, a T_2-weighted projection image was acquired (FOV = 70 mm, matrix = 128 × 128, repetition time = 4 s, echo time = 50 ms).

The pixel values of the ^{19}F and proton density projection images were divided by their respective receiver gain numbers. (The receiver gain for ^{19}F imaging was always set to the same value, which was the maximum possible for the scanner.) An ROI was drawn around the empty space (air) surrounding the tumor mass in the ^{19}F image to compute the mean and standard deviation of the image noise. Pixels whose ^{19}F signal did not exceed the mean noise level by at least 2 SDs were excluded from further analysis. It should be noted that the image noise in empty space (air) has a Rayleigh distribution with nonzero mean, which may differ from the noise distribution of the object in the image (37). Our simple calculations of the mean and standard deviation of the noise were not used for any analyses, only for thresholding. Pixels whose proton density signal was less than 10% of the maximum signal in the tumor

mass were also excluded. An estimate of the $[gem]_{rel}$ distribution (i.e., a $[gem]_{rel}$ image) was then obtained by dividing the ^{19}F image by the proton density image. The $[gem]_{rel}$ values for all images were then normalized to the average of the $[gem]_{rel}$ values for the control group, to facilitate comparisons.

RESULTS

Tumor Growth Experiments

The mice tolerated all treatments well, with no deaths and minimal weight loss (≤ 5%; drugs administered as in Table 1 group 1, then mice monitored daily with no further treatments up to 12 days postgemcitabine). Tumors in animals treated with gemcitabine grew more slowly than those in animals which were not treated with gemcitabine (8.1 ± 0.3 days vs 5.8 ± 0.3 days, n = 35 vs 35, $P < 0.0001$, all subgroups combined, where "days" refers to the number of days required for the tumor to grow from 8 mm [volume ~0.85 cm^3] to 15 mm [volume ~2.7 cm^3]). Among animals not treated with gemcitabine, there was no significant difference in tumor growth observed between subgroups. Among animals treated with gemcitabine, the results of the different subgroups are shown in Figure 1. There was no significant difference in tumor growth between the control subgroup (gemcitabine only) and the treatment (gemcitabine + modifier) subgroups, with the exception of BoNT-A. Tumors treated with gemcitabine plus BoNT-A grew more slowly than tumors treated with gemcitabine only (9.4 ± 0.6 days vs 7.7 ± 0.5 days, n = 9 vs 10, $P = 0.052$).

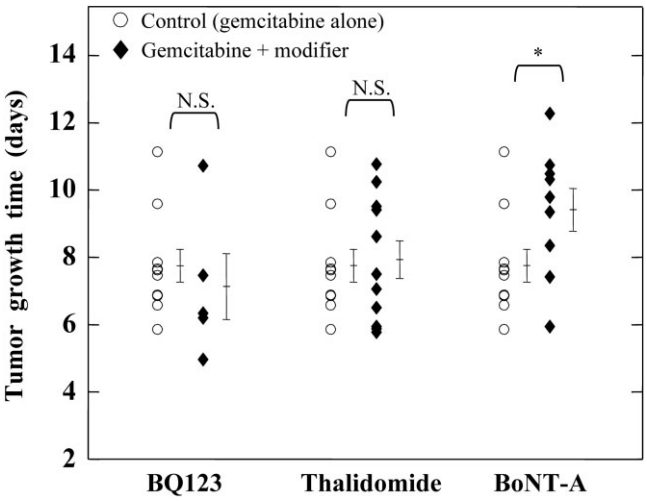

FIG. 1. Time for murine intramuscular hepatomas to grow to 15 mm diameter (volume ~2.7 cm^3; starting point = 8.0 ± 0.1 mm, volume ~0.85 cm^3). Thirty-five tumors (grown using the same cell suspension and same batch of mice) were divided into four experimental subgroups. The control subgroup (n = 10) was treated with gemcitabine 5 mg/kg alone. The other three subgroups were treated with gemcitabine plus a modifier (BQ123, n = 5; thalidomide, n = 11; and BoNT-A, n = 9). The results of the control group (circles) are shown next to the results of each modifier group for comparison. Vertical brackets to the right of each group show mean ± SEM for that group. N.S. = no significant difference between groups. * = significant difference between groups, student *t*-test, $P = 0.052$.

^{19}F and ^{1}H NMR Spectroscopy of Gemcitabine

Initial Uptake in Tumors In Vivo

Figure 2 shows example in vivo ^{19}F NMR spectra. Figure 3 shows the results of the ^{19}F spectroscopy initial uptake experiments. Similar to the tumor growth experiments, there was no significant difference in gemcitabine uptake between the control subgroups (gemcitabine only) and the treatment (gemcitabine + modifier) subgroups, with the exception of BoNT-A. Tumors treated with BoNT-A had a higher uptake of gemcitabine than controls (50% more, $P = 0.0008$). Additionally, there was no significant difference in $[gem]_{rel}$ between blood samples withdrawn from BoNT-A–treated mice and blood samples withdrawn from controls (2.9 ± 0.4 mM vs 3.2 ± 0.3 mM, where relative concentrations of gemcitabine were converted to estimates of absolute concentration by means of the scaling factor described in the Materials and Methods section). Finally, the estimate of the fraction of total NMR signal attributable to the tumor did not vary significantly between subgroups (MRI signal intensity from tumor volume divided by total MRI signal intensity = 0.63 on average).

Kinetics in Tumors In Vivo (BoNT-A Experiments)

Figure 4 shows the results of the gemcitabine kinetics experiments involving BoNT-A. For this figure, relative concentrations of gemcitabine were converted to absolute ones (mM) by means of the scaling factor described in the Materials and Methods section. The approximate symbol (~) has been placed in front of the mM symbol, however, because the conversion makes unverified assumptions of uniform distribution of gemcitabine, homogeneous unit density of tissue, and no NMR-invisible ^{1}H or ^{19}F nuclei. Tumors treated with BoNT-A received more gemcitabine over time than controls: The average AUC for the former subgroup was 40% higher than for the latter (356 ± 14 vs 252 ± 22, units of mM min, $P = 0.02$, Student *t*-test). No statistically significant difference in elimination rate was observed between the two subgroups (0.0025 ± 0.0005 mM/min for the control group vs 0.0038 ± 0.0011 mM/min for the BoNT-A group).

^{19}F MRI of Gemcitabine in Tumors In Vivo

Figure 5 shows example images from the ^{19}F imaging experiments. Pooling all $[gem]_{rel}$ values for all pixels of the treatment group (141 total pixels for the 5 animals) and comparing them with those of the control group (120 total pixels for the 4 animals), the $[gem]_{rel}$ values for the treatment group were significantly higher than those of the control group (1.21 ± 0.07 vs 1.00 ± 0.05, $P = 0.015$, Student *t*-test). Taking the average $[gem]_{rel}$ value for each image and comparing the two groups (5 $[gem]_{rel}$ values for the treatment group vs 4 $[gem]_{rel}$ values for the control group), the treatment group had higher $[gem]_{rel}$ values but the difference was not quite statistically significant (1.22 ± 0.10 vs 1.00 ± 0.05, $P = 0.1$).

DISCUSSION

The results of the initial uptake experiments closely matched those of the tumor growth experiments (compare

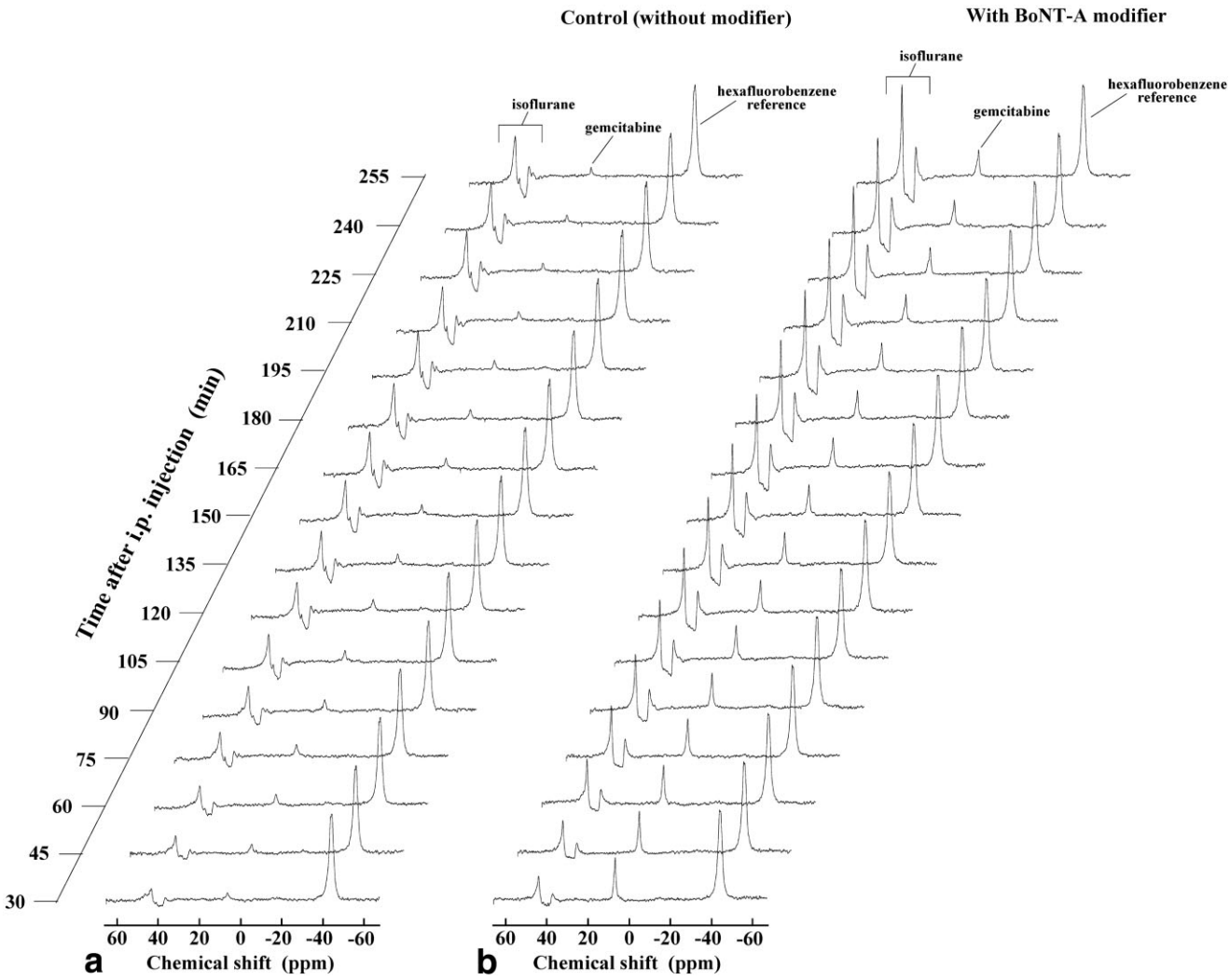

FIG. 2. Example in vivo ^{19}F NMR spectra for intramuscular hepatomas as a function of time after i.p. injection of gemcitabine 800 mg/kg. Identical scales have been used for all spectra. Each spectrum shows isoflurane peaks ($\sim +45$ ppm), the gemcitabine peak ($\sim +7$ ppm), and the hexafluorobenzene reference peak (~ -45 ppm). **a:** Spectra for a control tumor (no vascular modifiers administered). **b:** Spectra for a tumor pretreated with BoNT-A.

Figs. 1 and 3). Among the three modifiers, only BoNT-A showed a strong trend to enhance tumor growth inhibition by gemcitabine ($P = 0.052$) and gemcitabine uptake ($P = 0.0008$). Considering the results qualitatively, there appears to be the same trend in both figures whereby BQ123 is the least effective modifier, followed by thalidomide, followed by the most effective modifier BoNT-A. The results of the kinetics experiments in Figure 4 confirm that BoNT-A does indeed increase significantly the exposure of the tumor to gemcitabine (greater AUC, $P = 0.02$). Thus, it appears that the differences in gemcitabine chemosensitization for the three modifiers can be explained by corresponding differences in gemcitabine tumor uptake enhancement that they confer.

This study supports the assumption that ^{19}F NMR experiments can provide a reliable description of the pharmacokinetics of fluorinated chemotherapy drugs in tumors. In the context of the current work, these results suggest that ^{19}F NMR data can give a strong indication of the effectiveness of perfusion-enhancing vascular modifiers for improving gemcitabine chemotherapy in murine tumors.

At this time, it is not fully understood why the three modifiers affect gemcitabine uptake in tumors differently (and thus, chemosensitize differently). The data presented in this work are the first systematic, direct, comparison of the perfusion-enhancing and chemosensitization abilities of the three modifiers. Considering previously published data, however, it is possible to make some approximate comparisons of the three modifiers based upon laser Doppler imaging and Patent Blue staining (26–28,30). In the same tumor model, BQ123 and thalidomide were each found to cause an increase in laser Doppler-measured tumor blood flow of ~25% (relative to controls) (26,27). Thalidomide was found to increase the amount of tumor exposed to Patent Blue staining by ~70% (relative to controls) (27), whereas BoNT-A was found to increase the amount of tumor exposed to Patent Blue staining by

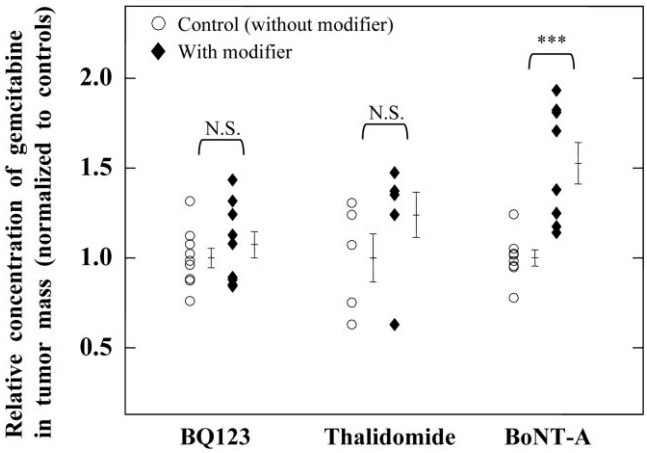

FIG. 3. Relative concentration of gemcitabine in tumor mass 45 min after i.p. injection of gemcitabine 800 mg/kg, as measured by in vivo NMR spectroscopy. Three different groups of murine intramuscular hepatomas, each subdivided into a control and modifier group, were investigated: BQ123 (n = 9 controls, 9 treated with modifier); thalidomide (n = 5 controls, 6 modifier); and BoNT-A (n = 8 controls, 8 modifier). For each of the three groups, relative gemcitabine concentrations (~mM) were normalized to the mean value found for the control group. Vertical brackets to the right of each group show mean ± SEM for that group. N.S. = no significant difference between groups. *** = highly significant difference between groups, student *t*-test, $P = 0.0008$.

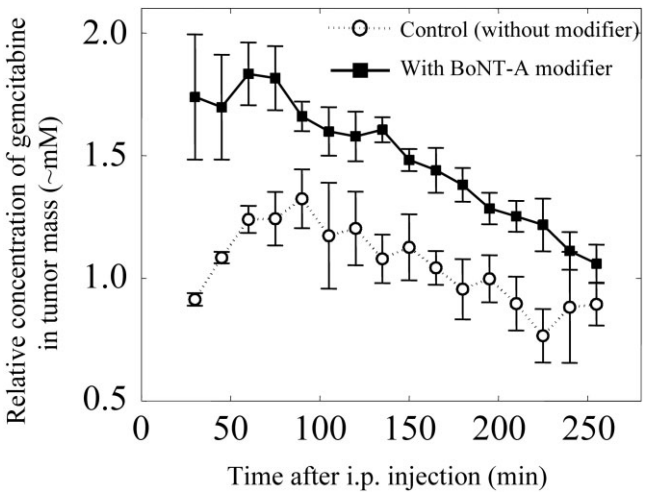

FIG. 4. Kinetics of the relative concentration of gemcitabine in the tumor mass after i.p. injection of gemcitabine 800 mg/kg, as measured by in vivo NMR spectroscopy. Six murine intramuscular hepatomas were subdivided into a control (n = 3) and BoNT-A modifier (n = 3) group. Data points (mean ± SEM) were obtained by averaging the concentrations from the three tumors of that group. The units of the vertical axis are absolute gemcitabine concentrations in millimolar (mM). For this figure, relative concentrations of gemcitabine were converted to absolute ones by means of the scaling factor described in the Materials and Methods section. The approximate symbol (~) has been placed in front of the mM symbol, however, because the conversion makes unverified assumptions of uniform distribution of gemcitabine, homogeneous unit density of tissue, and no NMR-invisible ^{1}H or ^{19}F nuclei.

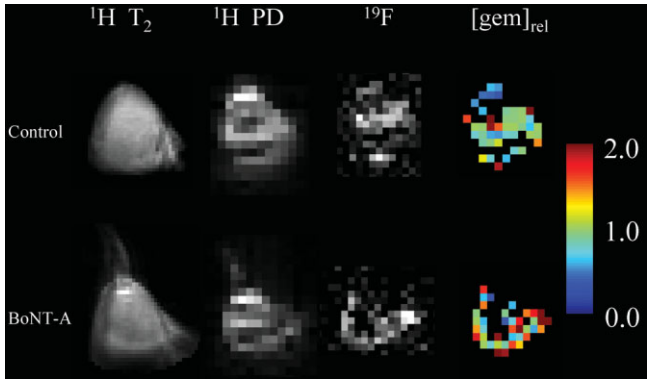

FIG. 5. Results of two murine intramuscular hepatoma imaging experiments. All images are projections (single-slice, ~infinite slice thickness) in the coronal plane (FOV = 7 cm, images cropped). Top row: a control study. Bottom row: a BoNT-A modifier study. Shown are 128 × 128 T_2-weighted ^{1}H images (leftmost column), 32 × 32 proton density-weighted ^{1}H images (second column), 32x32 ^{19}F images (third column), and 32 × 32 images of relative concentration of gemcitabine (rightmost column). Color scale shows relative concentration of gemcitabine. (Relative concentrations of gemcitabine have been normalized to the average value for the control group, to facilitate comparisons.)

~105% (30). This comparison of the three modifiers, although not rigorous, is consistent with the current study, where it was found that BoNT-A provided superior perfusion enhancement compared with the other two modifiers. Of note, our study does not exclude that thalidomide and BQ123 administered according to a different scheme (e.g., repeated exposure or higher dosage) might lead to a significant gain in chemotherapy uptake.

The dose of gemcitabine that was used for the in vivo ^{19}F spectroscopy tumor experiments (800 mg/kg) is higher than that used in similar work by previous investigators (e.g., 160 and 500 mg/kg for references 21 and 22). However, these previous studies used tumor models different from ours, did not report spectra SNR, and did not report estimates of absolute gemcitabine concentration in tumor, making comparisons with our work difficult. Relative to our ^{19}F spectroscopy acquisition parameters, the study performed with 160 mg/kg used a smaller spectral width (20 kHz), wider line broadening (40 Hz), longer acquisition times (30 min), and a shorter repetition time (1.5 s, which provides more FIDs and thus more averaging), all of which boost SNR (21). We used a long repetition time (6 s) to ensure complete spin-lattice relaxation of the ^{19}F nuclei, thus improving quantification. It should also be noted that the dose of 800 mg/kg used in our study is higher than that used for clinical human chemotherapy (~300–350 mg/kg equivalent for a 25-g mouse). It is expected that these clinical doses would still provide adequate SNR if ^{19}F NMR gemcitabine spectroscopy studies were performed on humans, especially given the typically large size of human tumors compared with murine tumors. We also note that, although a dose of 800 mg/kg caused no acute toxicity in our and other studies, we currently have no data on how such a high dose may affect tumor perfusion by means of either direct effects on tumor endothelium or nonspecific effects (36).

For the NMR spectroscopy experiments involving the initial uptake of gemcitabine, the relative concentration of gemcitabine was measured essentially at a single time point (45 min post-i.p.). From a pharmacokinetics viewpoint, it is better to measure the entire time course (e.g., from 0 to 250 min) and compute the AUC to obtain a measure of the exposure of the tumor to the drug. Compared with a single time point, the AUC is less affected by any potential animal-to-animal variations in the vascular input function and tumor pharmacokinetic parameters (e.g., tumor blood volume, capillary permeability, rates of cellular uptake and metabolism). AUC experiments are expensive, however, requiring large amounts of scanner time per animal. The strategy that we have envisioned is thus to use the single-time-point experiments as an initial "screening" test of the effectiveness of the vascular modifiers, followed up by AUC and ^{19}F imaging experiments if the results are promising. It should be kept in mind that, according to pharmacokinetic theory, it is possible for the results of single-time-point experiments to contradict those of AUC experiments, depending upon when the single time point is acquired. For the long-acting vascular modifiers used in this study (constant or gradually increasing effects with time constants ranging from hours to days), we believe that such a scenario is unlikely to have happened, especially considering the agreement with the tumor growth experiments.

We note that safety regulations prohibited us from handling chemotherapy drugs in the MRI laboratory, which prevented us from injecting gemcitabine while the animals were in the scanner (to obtain data starting at time 0). Collecting data from time 0 would not have changed the overall result of the BoNT-A AUC experiments (Fig. 4), however. This is because the control data (open circles) reached peak concentration at ~90 min. Pharmacokinetic theory would predict a smooth connection for the control data (i.e., relatively straight line) between 0 and 30 min, making it impossible for the AUC of the control data to exceed that of the BoNT-A data (filled squares).

Until now, few studies have attempted to obtain ^{19}F MR images of the distribution of fluorinated chemotherapy drugs, and none of these have demonstrated sufficient ^{19}F sensitivity to image individual tumors in any appreciable detail (23). Figure 5 shows ^{19}F MR images that we obtained of gemcitabine in tumors in vivo (spatial resolution = 2.2 mm). To our knowledge, these are the most detailed such images that have been published to date. There was a strong trend of higher $[gem]_{rel}$ values in the group treated with BoNT-A (P = 0.015 when all pixels are pooled into treatment vs control groups), which is consistent with the spectroscopy experiments. Moreover, we observed qualitatively a "ring" enhancement pattern (more gemcitabine in the periphery of the tumor compared with the center, e.g., Fig. 5 BoNT-A) in at least five of the nine tumors, which is consistent with tumor perfusion patterns often found with Gadolinium-enhanced MRI (38). Although these ^{19}F MRI results are very encouraging, the quality of the images still warrants improvement. It may be possible to increase the SNR of the images, for example, by acquiring the low-frequency components of the k-space lines (containing the most important image information) earlier in the free induction decay, thereby shortening the effective echo time.

CONCLUSIONS

The results of this study support the assumption that ^{19}F NMR experiments can provide a reliable description of the pharmacokinetics of fluorinated chemotherapy drugs in tumors. The results also show that ^{19}F NMR data can give a strong indication of the effectiveness of perfusion-enhancing vascular modifiers for improving gemcitabine chemotherapy in murine tumors. ^{19}F NMR is a promising tool for preclinical evaluation of such vascular modifiers and may ultimately be used in the clinic to monitor how these modifiers affect chemotherapy.

ACKNOWLEDGMENT

The authors thank Dr. Arturo Cardenas-Blanco for helpful discussions regarding statistical issues.

REFERENCES

1. van Laarhoven HW, Punt CJ, Kamm YJ, Heerschap A. Monitoring fluoropyrimidine metabolism in solid tumors with in vivo (19)F magnetic resonance spectroscopy. Crit Rev Oncol Hematol 2005;56:321–343.
2. Yu JX, Kodibagkar VD, Cui W, Mason RP. 19F: a versatile reporter for non-invasive physiology and pharmacology using magnetic resonance. Curr Med Chem 2005;12:819–848.
3. Martino R, Malet-Martino M, Gilard V. Fluorine nuclear magnetic resonance, a privileged tool for metabolic studies of fluoropyrimidine drugs. Curr Drug Metab 2000;1:271–303.
4. Robinson SP, Barton SJ, McSheehy PM, Griffiths JR. Nuclear magnetic resonance spectroscopy of cancer. Br J Radiol 1997;70:60–69.
5. van Laarhoven HW, Klomp DW, Kamm YJ, Punt CJ, Heerschap A. In vivo monitoring of capecitabine metabolism in human liver by 19fluorine magnetic resonance spectroscopy at 1.5 and 3 Tesla field strength. Cancer Res 2003;63:7609–7612.
6. Dzik-Jurasz AS, Collins DJ, Leach MO, Rowland IJ. Gallbladder localization of (19)F MRS catabolite signals in patients receiving bolus and protracted venous infusional 5-fluorouracil. Magn Reson Med 2000;44:516–520.
7. Wolf W, Presant CA, Waluch V. 19F-MRS studies of fluorinated drugs in humans. Adv Drug Deliv Rev 2000;41:55–74.
8. van Laarhoven HW, Gambarota G, Lok J, Lammens M, Kamm YL, Wagener T, Punt CJ, van der Kogel AJ, Heerschap A. Carbogen breathing differentially enhances blood plasma volume and 5-fluorouracil uptake in two murine colon tumor models with a distinct vascular structure. Neoplasia 2006;8:477–487.
9. McSheehy PM, Port RE, Rodrigues LM, Robinson SP, Stubbs M, van der Borns K, Peters GJ, Judson IR, Leach MO, Griffiths JR. Investigations in vivo of the effects of carbogen breathing on 5-fluorouracil pharmacokinetics and physiology of solid rodent tumours. Cancer Chemother Pharmacol 2005;55:117–128.
10. Kamm YJ, Peters GJ, Hull WE, Punt CJ, Heerschap A. Correlation between 5-fluorouracil metabolism and treatment response in two variants of C26 murine colon carcinoma. Br J Cancer 2003;89:754–762.
11. Kamm YJ, Heerschap A, Wagener DJ. Effect of carbogen breathing on the pharmacodynamics of 5-fluorouracil in a murine colon carcinoma. Eur J Cancer 2000;36:1180–1186.
12. Katzir I, Shani J, Wolf W, Chatterjee-Parti S, Berman E. Enhancement of 5-fluorouracil anabolism by methotrexate and trimetrexate in two rat solid tumor models, Walker 256 carcinosarcoma and Novikoff hepatoma, as evaluated by 19F-magnetic resonance spectroscopy. Cancer Invest 2000;18:20–27.
13. Lemaire LP, McSheehy PM, Griffiths JR. Pre-treatment energy status of primary rat tumours as the best predictor of response to 5-fluorouracil chemotherapy: a magnetic resonance spectroscopy study in vivo. Cancer Chemother Pharmacol 1998;42:201–209.
14. McSheehy PM, Robinson SP, Ojugo AS, Aboagye EO, Cannell MB, Leach MO, Judson IR, Griffiths JR. Carbogen breathing increases 5-fluorouracil uptake and cytotoxicity in hypoxic murine RIF-1 tumors: a magnetic resonance study in vivo. Cancer Res 1998;58:1185–1194.

15. McSheehy PM, Seymour MT, Ojugo AS, Rodrigues LM, Leach MO, Judson IR, Griffiths JR. A pharmacokinetic and pharmacodynamic study in vivo of human HT29 tumours using 19F and 31P magnetic resonance spectroscopy. Eur J Cancer 1997;33:2418–2427.
16. Holland SK, Bergman AM, Zhao Y, Adams ER, Pizzorno G. 19F NMR monitoring of in vivo tumor metabolism after biochemical modulation of 5-fluorouracil by the uridine phosphorylase inhibitor 5-benzylacyclouridine. Magn Reson Med 1997;38:907–916.
17. Blackstock AW, Kwock L, Branch C, Zeman EM, Tepper JE. Tumor retention of 5-fluorouracil following irradiation observed using 19F nuclear magnetic resonance spectroscopy. Int J Radiat Oncol Biol Phys 1996;36:641–648.
18. Kamm VJ, Rietjens IM, Vervoort J, Heerschap A, Rosenbusch G, Hofs HP, Wagener DJ. Effect of modulators on 5-fluorouracil metabolite patterns in murine colon carcinoma determined by in vitro 19F nuclear magnetic resonance spectroscopy. Cancer Res 1994;54:4321–4326.
19. Shungu DC, Bhujwalla ZM, Li SJ, Rose LM, Wehrle JP, Glickson JD. Determination of absolute phosphate metabolite concentrations in RIF-1 tumors in vivo by 31P–1H-2H NMR spectroscopy using water as an internal intensity reference. Magn Reson Med 1992;28:105–121.
20. McSheehy PM, Prior MJ, Griffiths JR. Prediction of 5-fluorouracil cytotoxicity towards the Walker carcinosarcoma using peak integrals of fluoronucleotides measured by MRS in vivo. Br J Cancer 1989;60:303–309.
21. Blackstock AW, Lightfoot H, Case LD, Tepper JE, Mukherji SK, Mitchell BS, Swarts SG, Hess SM. Tumor uptake and elimination of 2′,2′-difluoro-2′-deoxycytidine (gemcitabine) after deoxycytidine kinase gene transfer: correlation with in vivo tumor response. Clin Cancer Res 2001;7:3263–3268.
22. Kristjansen PE, Quistorff B, Spang-Thomsen M, Hansen HH. Intratumoral pharmacokinetic analysis by 19F-magnetic resonance spectroscopy and cytostatic in vivo activity of gemcitabine (dFdC) in two small cell lung cancer xenografts. Ann Oncol 1993;4:157–160.
23. Brix G, Bellemann ME, Haberkorn U, Gerlach L, Bachert P, Lorenz WJ. Mapping the biodistribution and catabolism of 5-fluorouracil in tumor-bearing rats by chemical-shift selective 19F MR imaging. Magn Reson Med 1995;34:302–307.
24. Brunstein F, Eggermont AMM, Aan de Wiel-Ambagtsheer G, Van Tiel ST, Rens J, Ten Hagen TLM. Synergistic antitumor effects of histamine plus melphalan in isolated hepatic perfusion for liver metastases. Ann Surg Oncol 2007;14:795–801.
25. Gupta N, Saleem A, Kotz B, Osman S, Aboagye EO, Phillips R, Vernon C, Wasan H, Jones T, Hoskin PJ, Price PM. Carbogen and nicotinamide increase blood flow and 5-fluorouracil delivery but not 5-fluorouracil retention in colorectal cancer metastases. Clin Cancer Res 2006;12:3115–3123.
26. Sonveaux P, Dessy C, Martinive P, Havaux X, Jordan BF, Gallez B, Gregoire V, Balligand JL, Feron O. Endothelin-1 is a critical mediator of myogenic tone in tumor arterioles: implications for cancer treatment. Cancer Res 2004;64:3209–3214.
27. Ansiaux R, Baudelet C, Jordan BF, Beghein N, Sonveaux P, De Wever J, Martinive P, Gregoire V, Feron O, Gallez B. Thalidomide radiosensitizes tumors through early changes in the tumor microenvironment. Clin Cancer Res 2005;11:743–750.
28. Segers J, Fazio VD, Ansiaux R, Martinive P, Feron O, Wallemacq P, Gallez B. Potentiation of cyclophosphamide chemotherapy using the anti-angiogenic drug thalidomide: importance of optimal scheduling to exploit the 'normalization' window of the tumor vasculature. Cancer Lett 2006;244:129–135.
29. Jain RK. Normalizing tumor vasculature with anti-angiogenic therapy: a new paradigm for combination therapy. Nat Med 2001;7:987–989.
30. Ansiaux R, Baudelet C, Cron GO, Segers J, Dessy C, Martinive P, De Wever J, Verrax J, Wauthier V, Beghein N, Gregoire V, Buc Calderon P, Feron O, Gallez B. Botulinum toxin potentiates cancer radiotherapy and chemotherapy. Clin Cancer Res 2006;12:1276–1283.
31. Carducci MA, Padley RJ, Breul J, Vogelzang NJ, Daliani DD, Schulman CC, Nabulsi AA, Humerickhouse RA, Weinberg MA, Schmitt JL, Nelson JB. Effect of endothelin-A receptor blockade with atrasentan on tumor progression in men with hormone-refractory prostate cancer: a randomized, phase II, placebo-controlled trial. J Clin Oncol 2003;21:679–689.
32. Michaelson MD, Kaufman DS, Kantoff P, Oh WK, Smith MR. Randomized phase II study on Atrensentan alone or in combination with zoledronic acid in men with metastatic prostate cancer. Cancer 2006;107:530–535.
33. Figg WD, Li H, Sissung T, Retter A, Wu S, Gulley JL, Arlen P, Wright JJ, Parnes H, Fedenko K, Latham L, Steinberg SM, Jones E, Chen C, Dahut W. Pre-clinical and clinical evaluation of estramustine, docetaxel and thalidomide combination in androgen-independent prostate cancer. Br J Urol 2007;99:1047–1055.
34. Klein AW. Complications, adverse reactions, and insights with the use of botulinum toxin. Dermatol Surg 2003;29:549–556
35. Taper HS, Woolley GW, Teller MN, Lardis MP. A new transplantable mouse liver tumor of spontaneous origin. Cancer Res 1966;26:143–148.
36. Fields MT, Eisbruch A, Normolle D, Orfali A, Davis MA, Pu AT, Lawrence TS. Radiosensitization produced in vivo by once- vs. twice-weekly 2′2′-difluoro-2′-deoxycytidine (gemcitabine). Int J Radiat Oncol Biol Phys 2000;47:785–791.
37. Gudbjartsson H, Patz S. The rician distribution of noisy MRI data. Magn Reson Med 1995;34:910–914.
38. Hayes C, Padhani AR, Leach MO. Assessing changes in tumour vascular function using dynamic contrast-enhanced magnetic resonance imaging. NMR Biomed 2002;15:154–163.